THE JOURNAL OF PHYSICAL CHEMISTRY A

Article

pubs.acs.org/JPCA

Structural Motifs of $[Fe(CO_2)_n]^-$ Clusters (n = 3−7)

Published as part of The Journal of Physical Chemistry virtual special issue "Veronica Vaida Festschrift".

Michael C. Thompson,[†] Leah G. Dodson,[‡] and J. Mathias Weber*[,†]

[†]JILA and Department of Chemistry and Biochemistry and [‡]JILA and NIST, University of Colorado, 440 UCB, Boulder, Colorado 80309-0440, United States

Supporting Information

ABSTRACT: We present IR spectra and quantum chemical calculations for anionic iron−CO_2 clusters of the form $[Fe(CO_2)_n]^-$ (n = 3−7). All observed clusters have at least two CO_2 units strongly bound to the metal atom. These strongly bound iron−CO_2 complexes form the core ions of the clusters and are solvated by additional, weakly bound CO_2 molecules. Larger clusters show clear infrared signatures of core ion isomers with three CO_2 moieties as well. Dominant structural motifs are based on bidentate CO_2 ligands with Fe−O/Fe−C bonds, oxalate ligands, and metal insertion into a CO bond.

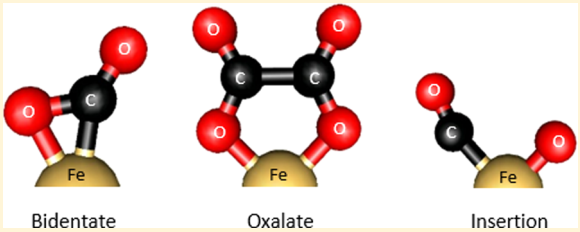

INTRODUCTION

The interaction of transition metals with CO_2 is of interest, both from a fundamental point of view[1,2] and in the context of CO_2 reduction by transition metal containing catalysts for CO_2 capture and sequestration[3] or recycling of CO_2 in a carbon-neutral fuel cycle.[4,5] In the context of CO_2 reduction on heterogeneous catalysts, the interaction of an under-coordinated metal atom with CO_2 in the presence of excess negative charge is of particular relevance, since heterogeneous electrocatalysts typically consist of atomically rough surfaces. These surfaces have many corner and edge sites, which are thought to be the catalytically active centers.[6]

It is difficult to determine the molecular-level mechanisms of CO_2 electroreduction catalysis in the condensed phase due to speciation, as electrochemical cells in operando present a very complicated chemical situation, and it is very challenging to disentangle the many overlapping signatures (spectroscopic or electrochemical) from such mixtures. For a thorough, fundamental understanding of the chemistry involved in the interaction of metals with small molecules, mass spectrometry-based ion chemistry experiments have been a particularly fruitful avenue.[7,8] Combining tandem mass spectrometry and laser spectroscopy to perform photodissociation spectroscopy of mass selected ions has been used as an even more powerful tool to examine the structure and charge distribution in metal−CO_2 complexes[9,10] and has led to a deeper understanding of metal−CO_2 interactions.

Infrared (IR) spectroscopy studies by several groups have found that the structures of cationic clusters of metal atoms with CO_2, $[M(CO_2)_n]^+$, are governed largely by electrostatic interaction of the metal cation with one of the oxygen atoms on the CO_2,[9,11−14] although in some cases electron transfer from the metal cation to the CO_2 solvent leads to the formation of CO_2 dimer anions, $(CO_2)_2^-$.[15] The character of the metal−CO_2 interactions in cationic clusters is reflected in the corresponding binding energies, which were determined by Armentrout and co-workers to be on the order of 0.6 eV.[16]

In contrast, all anionic $[M(CO_2)_n]^-$ clusters studied so far exhibit significant covalent bonding between the metal and at least one CO_2 ligand, resulting in the formation of M−C and M−O bonds. This results in a wide variety of structural motifs including metalloformates,[17−19] bidentate metal−CO_2 interaction,[20−22] and metal−oxalate ion pair formation.[17,23] In each case, a significant portion of the excess negative charge resides on the ligand(s) upon binding to the metal atom; in other words, the CO_2 ligand(s) are partially reduced. The core ions in clusters involving first-row transition metals mainly consist of CO_2 ligands binding in a bidentate fashion to the metal through the carbon and oxygen atoms.[20,21,23] In many cases, the charge distribution in the core ions depends on their solvation environment.

In this work we present IR photodissociation spectroscopy and quantum chemical calculations of mass selected $[Fe(CO_2)_n]^-$ (n = 3−7) and analyze and assign the dominant structural motifs in Fe−CO_2 bonding as a function of cluster size.

METHODS

Experimental Section. Details of our experimental setup have been published in previous work.[24,25] We generate Fe vapor via pulsed laser vaporization of a rotating Fe target with the third harmonic of a Nd:YAG laser (355 nm; 35 mJ/pulse; pulse duration 5−7 ns). The resulting Fe vapor is entrained into a pulsed supersonic expansion of CO_2 (stagnation pressure

Received: March 22, 2017
Revised: May 2, 2017
Published: May 12, 2017

DOI: 10.1021/acs.jpca.7b02742
J. Phys. Chem. A 2017, 121, 4132−4138

5.5 bar) by an Even−Lavie valve. This process generates several anionic species, including $(CO_2)_n^-$ and $[Fe(CO_2)_n]^-$. Anions are accelerated to ∼3.5 keV kinetic energy and are mass-separated in a Wiley−McLaren type time-of-flight mass spectrometer. After mass separation, ions are mass selected by a pulsed mass gate and then irradiated with the output of a tunable optical parametric converter system operating in the IR (we focus on the region of 975−2150 cm^{-1} in this work). Absorption of a photon with sufficient energy to overcome the binding energy of a weakly bound CO_2 solvent molecule will result in the loss of one CO_2 molecule with near unit probability. A reflectron is used as a secondary mass analysis step to mass separate undissociated parent ions from daughter ions generated by photodissociation. Photodissociation action spectra are measured by monitoring the formation of daughter ions as a function of photon energy, corrected for photon fluence.

Computational. Quantum chemical calculations were performed using the TURBOMOLE program package.[26] Cluster geometries were optimized employing density functional theory[27] (B3LYP functional)[28] with dispersion correction[29] and def2-TZVPP basis sets[30] for all atoms. Initial structures for calculations were generated using chemical intuition, based in part on previous studies of metal−CO_2 complexes.[17−23] Harmonic frequencies for all species were calculated using the AOFORCE program[31] and scaled by a factor of 0.975, derived from earlier work.[20] Simulated spectra were generated by convoluting the scaled calculated frequencies with a Gaussian (12 cm^{-1} full width at half-maximum, to match typical experimental line widths). The charge distribution in the complexes was characterized using Natural Population Analysis.[32]

We performed geometry optimizations and zero-point corrections using the PBE0 functional[33] to qualitatively assess the robustness of the relative energies of different isomers for n = 3, using the same basis sets as employed for the B3LYP calculations.

RESULTS AND DISCUSSION

Overview. Photodissocation action spectra for $[Fe(CO_2)_n]^-$ (n = 3−7) in the spectral range of 950−2150 cm^{-1} are shown in Figure 1. The features in these spectra are due to vibrational modes that are localized on the partially reduced CO_2 ligands belonging to the core ion. Excess electron density on CO_2 ligands results in a red shift of the CO stretching frequencies from their values in neutral CO_2 due to a weakening of the CO bonds, as the excess electron is accommodated in orbitals with overall antibonding character. These orbitals are analogous to the antibonding lowest unoccupied orbital of neutral CO_2. The presence of excess electron density on CO_2 ligands also results in an increase of the CO bond distance by ∼8% (from 115 pm in free neutral CO_2 to 124 pm in the anion) and in a substantial decrease of the OCO bond angle. The extent of the observed red shift can be correlated to the amount of charge on the CO_2 ligand as shown by photodissociation spectroscopy performed on $[M(CO_2)_n]^-$ (M = Au, Ag, Cu, Bi) clusters.[17−19,23] For simplicity, we will refer to CO_2 moieties that are part of the core ions as ligands, in contrast to CO_2 molecules that take the role of solvent molecules.

Exploratory measurements in the spectral range of 2200−2400 cm^{-1} showed a single feature for each cluster size (n = 3−7) between 2341 and 2345 cm^{-1}. This feature is due to the antisymmetric stretching motions of the nominally neutral solvent CO_2 molecules,[34] which are very slightly red-shifted from the position in free CO_2 (at 2349 cm^{-1}, see Supporting Information) due to the presence of the negative charge. These features did not change significantly as a function of cluster size, but their presence implies that at least one of the CO_2 molecules played the role of a solvent for each cluster size. It is important to note that no IR photodissociation signal was found in any spectral region for clusters smaller than n = 3.

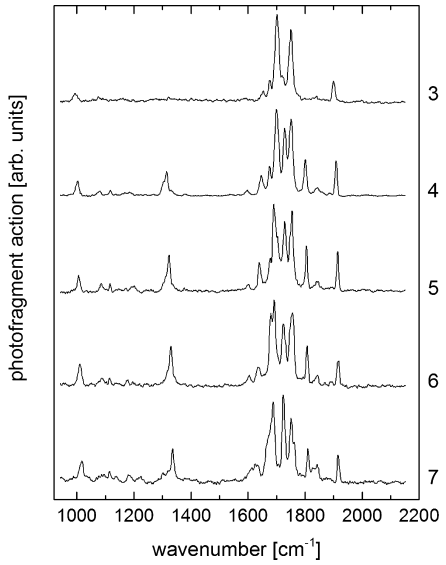

Figure 1. Photodissociation action spectra of $[Fe(CO_2)_n]^-$ (n = 3−7) in the CO stretching region of the core ions. Numbers on the right indicate the cluster size.

To interpret the spectra, some insight regarding the energy dependence of the photodissociation efficiency is necessary, and the observation of solvent signatures is significant in this context. The binding energy of a solvent CO_2 molecule to the various core ion candidate structures in the present work is calculated to be ca. 1500 cm^{-1} or lower. In contrast, CO_2 ligands have calculated binding energies in excess of 4000 cm^{-1}, and can in fact be of the order of 1×10^4 cm^{-1}. We note that the core ion interaction with the solvent is mainly electrostatic. On the basis of a comparison with experimental thermodynamic data on $[Fe\text{-}CO_2]^+$,[16] our calculations slightly overestimate the binding energy of solvent molecules (ca. 20%) but yield overall reasonable energies. Since our experiment relies on photodissociation as a means to detect photon absorption, it is important to note that we cannot photodissociate the core ions themselves with a single IR photon. As a result, a core ion must be solvated by at least one CO_2 solvent molecule for its photodissociation spectrum to be observable in our experiment. This immediately eliminates the ability to measure the IR spectrum of a bare $[FeCO_2]^-$ complex. By the same argument, in the case of clusters of composition $[Fe(CO_2)_2]^-$, the experiment is only sensitive to laser-induced dissociation from clusters of the form $[FeCO_2]^-\cdot CO_2$. Experiments on this cluster size showed no laser-induced loss of a CO_2 unit, implying that all core ions at this cluster size have two strongly bound CO_2 ligands. This highlights the high affinity that Fe must have for CO_2 molecules in the presence of an excess electron, since no solvated complexes with fewer than two CO_2 ligands appear to be formed in our molecular beam. We can therefore expect that the smallest core ion in $[Fe(CO_2)_3]^-$ cluster ions has the stoichiometry $[Fe(CO_2)_2]^-$.

DOI: 10.1021/acs.jpca.7b02742
J. Phys. Chem. A 2017, 121, 4132−4138

Just as the high dissociation energy of the core ion precludes one-photon photodissociation in the IR spectral region under study, the binding energy of the solvent molecules is important for the dissociation probability upon photon absorption. Assuming that the clusters in our ion source are formed as an evaporative ensemble, which is typical for a supersonic expansion, the average internal energy of a cluster is on the order of the binding energy of the last particle that was evaporated during cluster formation in the ion source.[35] This energy can be estimated to be similar to the binding energy of the CO_2 solvent molecules in the cluster. If the energy of an absorbed photon is greater than the binding energy of a solvent CO_2 molecule, the cluster will dissociate upon photon absorption with quantum yields close to unity. If the photon energy is less than the binding energy of a CO_2 solvent molecule, the cluster can still fragment, but the dissociation process must be assisted by the thermal energy content of the cluster prior to irradiation. The quantum yield for this process decreases significantly with decreasing photon energy, and the experimentally observable features will be suppressed for photon energies below the binding energy of a solvent CO_2 molecule.

$[Fe(CO_2)_3]^-$. The spectrum for $[Fe(CO_2)_3]^-$ shows several peaks between 1650 and 1750 cm^{-1}, as well as several features below 1300 cm^{-1} and a feature at 1900 cm^{-1}. The calculated structures and their relative energies for this cluster size are shown in Figure 2. Anionic complexes of a single iron atom with multiple CO_2 molecules may exist in a doublet or quartet configuration. Our calculations show consistently that structures with quartet spin are lower in energy, on average by 1 eV, than structures with the same connectivity and doublet spin. Ions that may have formed in a doublet state can simply relax by a spin flip (i.e., without a large geometry change), and other metal−organic iron complexes have intersystem crossing lifetimes in the microsecond range and shorter.[36] It seems unlikely that they will survive the time between ion formation and irradiation (milliseconds). This suggests that all complexes arriving in the laser interaction region have quartet configurations.

We assign the two prominent bands in the spectrum of $[Fe(CO_2)_3]^-$ at 1699 and 1749 cm^{-1} to the antisymmetric CO stretching vibrations of the CO_2 ligands in structure B(1a) or B(1b). This structural family features two strongly bound CO_2 bidentate ligands, each bound to the metal with the carbon and an oxygen atom. This "butterfly" type of core ion is planar and has C_{2v} symmetry. Similar, but nonplanar structures have been previously observed with nickel and cobalt as the metal center.[20,21] Charge analysis of the bare complex shows that each of the two CO_2 ligands has a charge of −0.89 e. Kinetic coupling of the CO oscillators across the two CO_2 ligands yields in-phase and out-of-phase combinations of the individual CO_2 asymmetric stretching modes. We assign the higher energy feature (1749 cm^{-1}) to the in-phase combination and the lower energy feature (1699 cm^{-1}) to the out-of-phase combination. Calculated spectra for butterfly-type structures (see Figure 3) show a third high-intensity feature predicted at 1042 cm^{-1}, which is the signature of the out-of-phase combination of symmetric CO stretching motions. As discussed above, the low energy of this feature results in significant suppression in the experimental spectrum, due to the binding energy of the solvent CO_2 to this core ion geometry (1400 cm^{-1}). With this suppression effect in mind, we assign the peak at 993 cm^{-1} in the experimental spectrum to the out-of-phase combination of the symmetric CO stretching modes of the two CO_2 ligands.

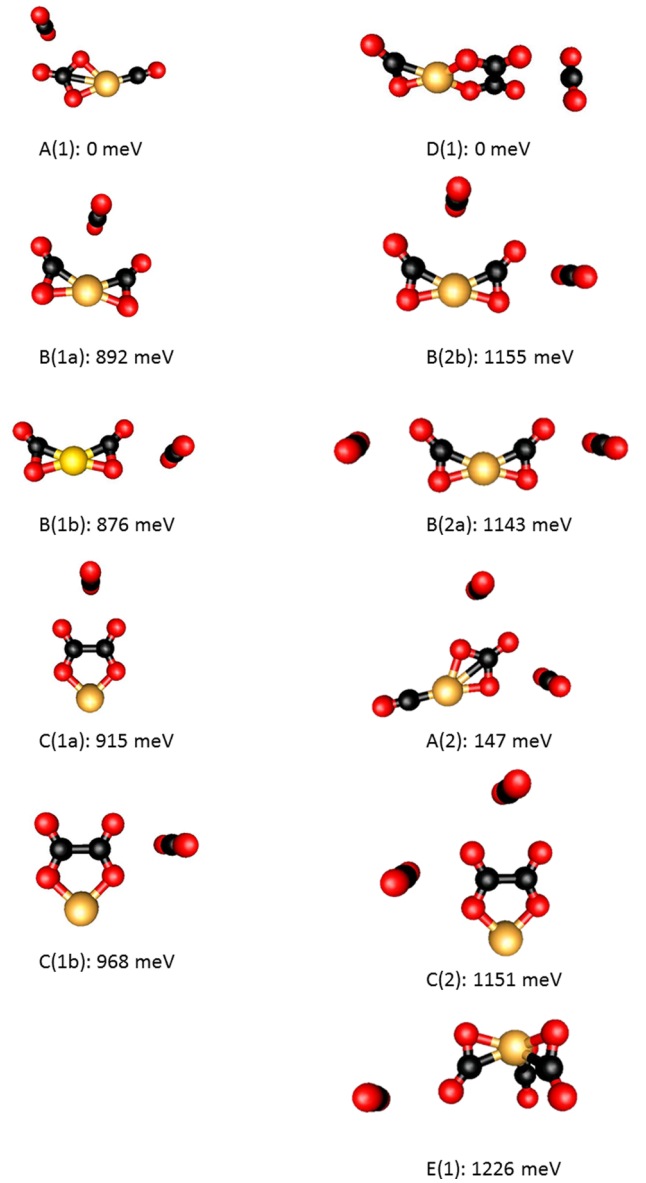

Figure 2. Calculated structures of $Fe(CO_2)_3^-$ (left) and $Fe(CO_2)_4^-$ (right). Structures are labeled based on structural motif (capital letters), the number of solvent molecules (numbers), and solvent conformation (lowercase letters). All structures are calculated with quartet spin. Calculations for n = 3 with the PBE0 functional reproduce the relative energies as shown (within 70 meV).

Since the excess electron density on the CO_2 ligands weakens the CO bonds, the calculated CO bond distance is greater than in neutral CO_2, increasing from 115 pm in the neutral to 130 and 120 pm for the metal-bound CO bond and the free CO bond, respectively. This also results in a decrease of the OCO bond angle of the solvated ligand from 180° to 130°. The change in angle can be qualitatively understood based on the Walsh diagram of CO_2,[37] which shows that the orbital accommodating an excess electron in CO_2 is stabilized by decreasing the OCO angle, and this behavior is retained in CO_2 functional groups.

The butterfly complex has several different binding sites for solvation. In particular, the solvent can be symmetric with

DOI: 10.1021/acs.jpca.7b02742
J. Phys. Chem. A 2017, 121, 4132−4138

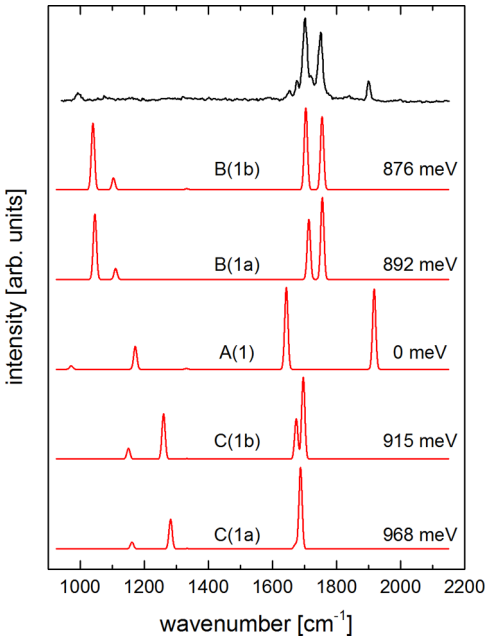

Figure 3. Comparison of calculated (lower traces, red) IR spectra to experimental (top trace, black) spectrum of $[Fe(CO_2)_3]^-$.

respect to the two CO_2 ligands [B(1a)], or it can interact with only one of the ligands [B(1b)]. A CO_2 solvent molecule in an asymmetric solvation conformer polarizes the molecular charge toward the solvated side of the complex. This leads to a ca. 5% increase in the charge of the solvated ligand and a concomitant decrease of the charge in the opposite ligand by approximately the same amount. The charge asymmetry also breaks the symmetry of the core ion and leads to a difference between the force constants of the CO bonds of the two ligands. As a result, the calculations predict a red shift of the out-of-phase combination and a blue shift of the in-phase combination, as well as a change in the relative intensities of the two features (see Figure 3).

The feature at 1898 cm^{-1} is not recovered by a butterfly core ion structure and strongly suggests the presence of a different structural family. The frequency either points to a weakly reduced CO_2 ligand or to a CO group bound to the metal. The presence of a CO group bound to the metal would require that the metal insert itself into one of the CO bonds of CO_2. Such a process should have a very high reaction barrier (see Figure 4), even though it results in the lowest-energy isomer. Different from the other first-row transition-metal complexes with CO_2 investigated in our group,[20,21] this characteristic signature for isomer A(1) bears significant intensity, and we assign the band at 1898 cm^{-1} to the lone CO stretching motion of structure A(1). We note that there is a second feature predicted for this structure, calculated at 1646 cm^{-1}, which can be characterized by an asymmetric stretching mode of the CO_3 ligand. This signature is likely reflected in one of the two small shoulders to the red of the two dominant peaks, although the accuracy of our calculations does not allow a definitive assignment. Similar to the discussion involving isomer B, we expect the features predicted for isomer A below 1500 cm^{-1} to be suppressed due to kinetic shift effects associated with the binding energy of a solvent CO_2 molecule, and the lower-energy experimental feature of isomer A is likely too weak to be observed in our experiment, at least at this cluster size.

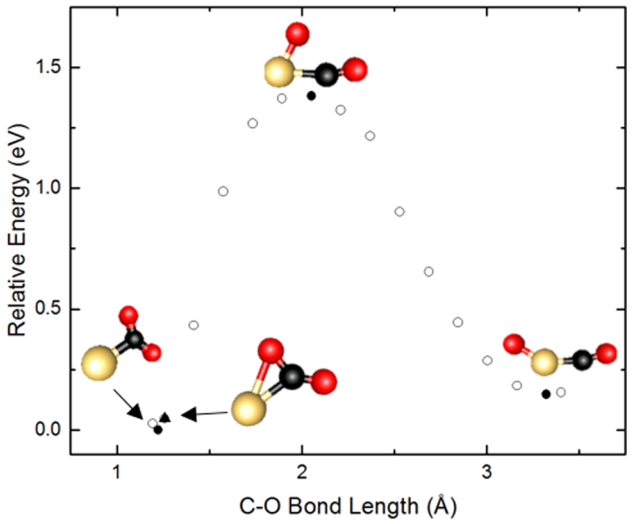

Figure 4. Potential energy surface for insertion of Fe into a CO bond in $FeCO_2^-$. The barrier was found by scanning one of the two CO bond distances, while all other coordinates were allowed to relax. The filled symbols correspond to the structures shown. The calculated barrier height is 1.38 eV.

Calculations also predict an oxalate complex as a viable isomer of the core ion. Structures C(1a) and C(1b) could account for one of the low-intensity shoulders in the experimental spectrum around the most intense peak, although our calculations do not allow us to pinpoint which of the two weak candidate peaks in the spectrum belong to this isomer family. This feature can be characterized as the in-phase combination of asymmetric stretching motions of the two CO_2 subunits. In the calculated spectra for core ion C, we note that both the frequency and the relative intensity of the in-phase and out-of-phase asymmetric stretching combinations are affected by the location of the weakly bound solvent molecule. When the oxalate ligand is solvated symmetrically [C(1a)], the out-of-phase mode is predicted to be nearly IR inactive; that is, there is only a very small transition dipole moment for this mode. However, when the presence of the solvent molecule breaks the symmetry of the complex [C(1b)], there is a significant intensity enhancement of this mode. This effect is also reflected in the charge distribution of the complex under symmetric solvation (−0.84 e per CO_2 moiety) compared to asymmetric solvation (−0.86 e in the solvated CO_2 moiety vs −0.83 e in the bare moiety). The change in the charge distribution of the oxalate ligand also induces weak geometry changes in the individual CO_2 moieties. Under symmetric solvation, each CO_2 moiety has an OCO bond angle of 124.7°, while under asymmetric solvation the solvated CO_2 moiety has an OCO bond angle of 123.9°, and the OCO bond angle on the other CO_2 moiety is nearly unchanged (124.8°). While the presence of the oxalate isomer at this cluster size is not unambiguously clear, it is certainly a candidate for some of the features observed in the spectrum. We will revisit isomers involving an oxalate ligand in the discussion of the larger clusters.

The relative energies of the calculated structures and their population warrant further discussion (see Table 1). Based solely on the relative energies, one would expect that core ion A would be the only populated isomer, since thermal population of the higher energy core ion isomers would require very high temperatures, and the cluster would not be able to retain

DOI: 10.1021/acs.jpca.7b02742
J. Phys. Chem. A 2017, 121, 4132−4138

Table 1. Comparison of Core Ion Energies

isomer[a]	rel energy[b] [meV]	isomer[c]	rel energy[b] [meV]
A(0)	0	A(1)	0
B(0)	906	B(1a)	892
C(0)	780	C(1a)	915
		D(0)	−207
		E(0)	918

[a]The left two columns show a comparison of the bare core ions with of the stoichiometry $[FeC_2O_4]^-$ (isomers A, B, and C). [b]All energies are relative to isomer A for each cluster size. [c]The right columns compare the energies of the unsolvated core ions with stoichiometry $[FeC_2O_6]^-$ isomers with singly solvated isomers A, B, and C.

weakly bound CO_2 solvent molecules. However, as mentioned before, the formation of the insertion structure requires the breaking of a CO bond, which leads to a high reaction barrier toward the formation of this species (see Figure 4). This reaction barrier allows clusters to become kinetically trapped in higher-energy isomers during the ion formation process, assuming that the collisional cooling rate during the supersonic expansion is greater than the isomerization rates for the relevant pathways. The presence of the butterfly and (potentially) oxalate vibrational features in the experimental spectrum confirms the hypothesis that a significant part of the population is kinetically trapped in higher-energy isomers in our experiment, consistent with the behavior of other metal−CO_2 clusters.[21,23]

$[Fe(CO_2)_4]^-$ and Larger Clusters. As mentioned above, our experimental strategy relies on the presence of a weakly bound solvent molecule for the detection of photon absorption. For the case of $n = 3$ we are therefore blind to core ions with three ligands, but if such core ions exist, their signatures should be observable in the experimental spectrum for $n = 4$. Comparison of the experimental spectrum of $[Fe(CO_2)_4]^-$ with the calculated spectra of structures shown in Figure 2 shows that some of the same core ion isomers are populated as in $[Fe(CO_2)_3]^-$ (see Figure 5). The signatures of the butterfly complex (B) and of the insertion structure (A) are clearly still present, although they are slightly shifted. However, several new features appear in the spectrum of $[Fe(CO_2)_4]^-$. The total number of spectral features suggests that several isomers are present as kinetically trapped species, similar to $[Fe(CO_2)_3]^-$.

The calculated spectra of the structures shown in Figure 2 can be used to describe the experimental spectrum and account for all major peaks. Structure D(1) is the lowest-energy structure at this cluster size. This finding is consistent with the relative energies of the bare core ion structures for isomers D and E, compared to singly solvated isomers A, B, and C (see Table 1). Core ion D can be characterized as a combination of a bidentate CO_2 ligand and an oxalate ligand, in other words, by addition of a bidentate CO_2 ligand to the oxalate complex (C). On the basis of the calculated spectrum of structure D(1), we assign the new spectral feature at 1799 cm^{-1} to the asymmetric stretching motion of the bidentate CO_2 ligand in this complex. The new feature at 1313 cm^{-1} corresponds to a breathing mode of the ring formed by the iron atom and the oxalate ligand in isomers C and D. Analysis of the charge distribution and structure of isomer D reveals that the addition of a bidentate ligand to the oxalate complex breaks the symmetry of the charge distribution in the oxalate ligand. The total charge on the oxalate ligand in isomer D is lower than in structure C, indicating that charge is shared between the oxalate and the

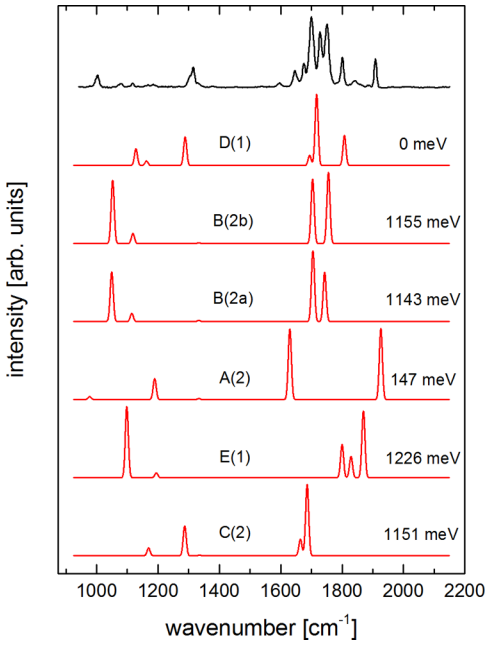

Figure 5. Comparison of calculated (lower traces, red) IR spectra to experimental (top trace, black) spectrum of $[Fe(CO_2)_4]^-$.

bidentate ligand, as expected. This is reflected in the calculated IR spectrum, as the characteristic frequencies of both the bidentate and the oxalate ligands are blue-shifted from the values in both the butterfly structure (B) and the oxalate complex (C). This shift is particularly strong for the antisymmetric CO stretching mode of the bidentate ligand at 1799 cm^{-1}, which is an unusually high frequency for this structural motif. The relatively low excess charge in the bidentate ligand (−0.68 e) is consistent with this shift. We note that the core ion in complex D(1) is not planar, as the bidentate CO_2 ligand is twisted out of the oxalate plane by ∼8°.

Another unique core ion geometry with three CO_2 ligands is the tris-bidentate geometry (E). This structure features three CO_2 molecules bound to the metal through metal−carbon and metal−oxygen bonds, and the resulting complex has C_{3v} symmetry. In the bare complex, the individual bidentate CO_2 ligands lie 120° apart, but upon solvation the entire complex is skewed toward the solvent molecule. The calculated vibrational spectrum of structure E(1) is consistent with the low-intensity features found in the experimental spectrum from 1800 to 1900 cm^{-1}.

For larger clusters, small spectral shifts of some of the features discussed above are observed with increasing cluster size, but no new spectral features appear. This suggests that there are no core ions larger than $[Fe(CO_2)_3]^-$ and that no new core ion geometries are at play.

The spectral signatures of $[Fe(CO_2)_n]^-$ clusters and the corresponding core ion structures are reminiscent of the results for other first-row transition metals in anionic clusters with CO_2. In particular, the bidentate and oxalate ligand motifs seem to give rise to the governing structural families for these metals, in contrast to the metalloformate ($MCOO^-$) structures that have emerged as the dominant motif for the later coinage metals (Ag, Au) and bismuth,[17−19] and whose connectivity is characterized by a weak M−C σ bond.

DOI: 10.1021/acs.jpca.7b02742
J. Phys. Chem. A 2017, 121, 4132−4138

CONCLUSIONS

The IR spectroscopy of $[Fe(CO_2)_n]^-$ cluster ions reveals rich structural diversity compared to analogous clusters based on cobalt or nickel. Similar to other anionic complexes of first-row transition metals with CO_2, there are no core ions with fewer than two CO_2 ligands in these clusters. Bidentate CO_2 ligands establishing Fe−C and Fe−O bonds to the metal atom are a dominant structural motif, but we also observe clear infrared spectroscopic signatures of oxalate ligands as well as characteristic features of metal-inserted structures that result in the formation of CO and CO_3 ligands. The infrared spectra of the clusters do not change significantly for $n > 4$, indicating that the observed isomers are robust, and increasing solvation with CO_2 does not change the binding motifs.

ASSOCIATED CONTENT

Supporting Information

The Supporting Information is available free of charge on the ACS Publications website at DOI: 10.1021/acs.jpca.7b02742.

Experimental spectra of $[Fe(CO_2)_n]^-$ cluster ions in the region of the solvent signatures; coordinates of the calculated minimum-energy structures of $[Fe(CO_2)_n]^-$ clusters for $n = 3$ and 4; mass spectrum of $[Fe(CO_2)_n]^-$ cluster ions and other species in the same mass range (PDF)

AUTHOR INFORMATION

Corresponding Author

*E-mail: weberjm@jila.colorado.edu. Phone: +1-303-492-7841.

ORCID

J. Mathias Weber: 0000-0002-5493-5886

Notes

The authors declare no competing financial interest.

ACKNOWLEDGMENTS

We gratefully acknowledge funding from the National Science Foundation (NSF) through the NSF AMO Physics Frontier Center at JILA (PHY-1125844). We also acknowledge graduate student support from the U.S. Department of Education through a GAANN Fellowship for M.C.T. This research was performed while L.G.D. held an NRC Research Associateship award at NIST.

REFERENCES

(1) Schwarz, H. Metal-mediated activation of carbon dioxide in the gas phase: Mechanistic insight derived from a combined experimental/computational approach. *Coord. Chem. Rev.* **2017**, *334*, 112−123.

(2) Gibson, D. H. The organometallic chemistry of carbon dioxide. *Chem. Rev.* **1996**, *96*, 2063−2095.

(3) Yang, H. Q.; Xu, Z. H.; Fan, M. H.; Gupta, R.; Slimane, R. B.; Bland, A. E.; Wright, I. Progress in carbon dioxide separation and capture: A review. *J. Environ. Sci.* **2008**, *20*, 14−27.

(4) Rosen, B. A.; Salehi-Khojin, A.; Thorson, M. R.; Zhu, W.; Whipple, D. T.; Kenis, P. J. A.; Masel, R. I. Ionic liquid-mediated selective conversion of CO_2 to CO at low overpotentials. *Science* **2011**, *334*, 643−644.

(5) Qiao, J.; Liu, Y.; Hong, F.; Zhang, J. A review of catalysts for the electroreduction of carbon dioxide to produce low-carbon fuels. *Chem. Soc. Rev.* **2014**, *43*, 631−675.

(6) Chen, Y.; Li, C. W.; Kanan, M. W. Aqueous CO_2 reduction at very low overpotential on oxide-derived Au anoparticles. *J. Am. Chem. Soc.* **2012**, *134*, 19969−19972.

(7) Böhme, D. K.; Schwarz, H. Gas-phase catalysis by atomic and cluster metal ions: The ultimate single-site catalysts. *Angew. Chem., Int. Ed.* **2005**, *44*, 2336−2354.

(8) Schröder, D.; Schwarz, H.; Clemmer, D. E.; Chen, Y. M.; Armentrout, P. B.; Baranov, V. I.; Böhme, D. K. Activation of hydrogen and methane by thermalized FeO^+ in the gas phase as studied by multiple mass spectrometric techniques. *Int. J. Mass Spectrom. Ion Processes* **1997**, *161*, 175−191.

(9) Walker, N. R.; Walters, R. S.; Duncan, M. A. Infrared photodissociation spectroscopy of $V^+(CO_2)_n$ and $V^+(CO_2)_nAr$ complexes. *J. Chem. Phys.* **2004**, *120*, 10037−10045.

(10) Boese, A. D.; Schneider, H.; Gloess, A. N.; Weber, J. M. The infrared spectrum of $Au^-\cdot CO_2$. *J. Chem. Phys.* **2005**, *122*, 154301.

(11) Walker, N. R.; Walters, R. S.; Grieves, G. A.; Duncan, M. A. Growth dynamics and intracluster reactions in $Ni^+(CO_2)_n$ complexes via infrared spectroscopy. *J. Chem. Phys.* **2004**, *121*, 10498−10507.

(12) Walters, R. S.; Brinkmann, N. R.; Schaefer, H. F.; Duncan, M. A. Infrared photodissociation spectroscopy of mass-selected $Al^+(CO_2)_n$ and $Al^+(CO_2)_nAr$ clusters. *J. Phys. Chem. A* **2003**, *107*, 7396−7405.

(13) Gregoire, G.; Velasquez, J.; Duncan, M. A. Infrared photodissociation spectroscopy of small Fe^+-$(CO_2)_n$ and Fe^+-$(CO_2)_n$ Ar clusters. *Chem. Phys. Lett.* **2001**, *349*, 451−457.

(14) Iskra, A.; Gentleman, A. S.; Kartouzian, A.; Kent, M. J.; Sharp, A. P.; Mackenzie, S. R. Infrared spectroscopy of gas-phase $M^+(CO_2)_n$ (M = Co, Rh, Ir) ion−molecule complexes. *J. Phys. Chem. A* **2017**, *121*, 133−140.

(15) Ricks, A. M.; Brathwaite, A. D.; Duncan, M. A. IR spectroscopy of gas phase $V(CO_2)_n^+$ clusters: solvation-induced electron transfer and activation of CO_2. *J. Phys. Chem. A* **2013**, *117*, 11490−11498.

(16) Tjelta, B. L.; Walter, D.; Armentrout, P. B. Determination of weak Fe^+−L bond energies (L = Ar, Kr, Xe, N_2, and CO_2) by ligand exchange reactions and collision-induced dissociation. *Int. J. Mass Spectrom.* **2001**, *204*, 7−21.

(17) Thompson, M. C.; Ramsay, J.; Weber, J. M. Solvent-driven reductive activation of CO_2 by bismuth: switching from metal-loformate complexes to oxalate products. *Angew. Chem., Int. Ed.* **2016**, *55*, 15171−15174.

(18) Knurr, B. J.; Weber, J. M. Solvent-mediated reduction of carbon dioxide in anionic complexes with silver atoms. *J. Phys. Chem. A* **2013**, *117*, 10764−10771.

(19) Knurr, B. J.; Weber, J. M. Solvent-driven reductive activation of carbon dioxide by gold anions. *J. Am. Chem. Soc.* **2012**, *134*, 18804−18808.

(20) Knurr, B. J.; Weber, J. M. Infrared spectra and structures of anionic complexes of cobalt with carbon dioxide ligands. *J. Phys. Chem. A* **2014**, *118*, 4056−4062.

(21) Knurr, B. J.; Weber, J. M. Interaction of nickel with carbon dioxide in $[Ni(CO_2)_n]^-$ clusters studied by infrared spectroscopy. *J. Phys. Chem. A* **2014**, *118*, 8753−8757.

(22) Knurr, B. J.; Weber, J. M. Structures of $CoO(CO_2)_n^-$ and $NiO(CO_2)_n^-$ clusters studied by infrared spectroscopy. *J. Phys. Chem. A* **2015**, *119*, 843−850.

(23) Knurr, B. J.; Weber, J. M. Structural diversity of copper-CO_2 complexes: infrared spectra and structures of $Cu(CO_2)_n^-$ clusters. *J. Phys. Chem. A* **2014**, *118*, 10246−10251.

(24) Weber, J. M.; Schneider, H. Infrared spectra of $X^-\cdot CO_2\cdot Ar$ cluster anions (X= Cl,Br,I). *J. Chem. Phys.* **2004**, *120*, 10246−10251.

(25) Weber, J. M. A pulsed ion source for the preparation of metal containing cluster ions using supersonic entrainment of laser vaporized metal. *Rev. Sci. Instrum.* **2005**, *76*, 043301.

(26) Ahlrichs, R.; Bär, M.; Häser, M.; Horn, H.; Kölmel, C. Electronic-structure calculations on workstation computers - the program system Turbomole. *Chem. Phys. Lett.* **1989**, *162*, 165−169.

(27) Parr, R. G.; Yang, W. *Density-Functional Theory of Atoms and Molecules;* Oxford University Press: New York, 1989.

(28) Lee, C. T.; Yang, W. T.; Parr, R. G. Development of the Colle-Salvetti correlation-energy formula into a functional of the electron-density. *Phys. Rev. B: Condens. Matter Mater. Phys.* **1988**, *37*, 785−789.

DOI: 10.1021/acs.jpca.7b02742
J. Phys. Chem. A 2017, 121, 4132−4138

(29) Grimme, S. Semiempirical GGA-type density functional constructed with a long-range dispersion correction. *J. Comput. Chem.* **2006**, *27*, 1787−1799.
(30) Weigend, F.; Ahlrichs, R. Balanced basis sets of split valence, triple zeta valence and quadruple zeta valence quality for H to Rn: Design and assessment of accuracy. *Phys. Chem. Chem. Phys.* **2005**, *7*, 3297−3305.
(31) Deglmann, P.; Furche, F.; Ahlrichs, R. An efficient implementation of second analytical derivatives for density functional methods. *Chem. Phys. Lett.* **2002**, *362*, 511−518.
(32) Reed, A. E.; Weinstock, R. B.; Weinhold, F. Natural population analysis. *J. Chem. Phys.* **1985**, *83*, 735−746.
(33) Perdew, J. P.; Ernzerhof, M.; Burke, K. Rationale for mixing exact exchange with density functional approximations. *J. Chem. Phys.* **1996**, *105*, 9982−9985.
(34) Shin, J. W.; Hammer, N. I.; Johnson, M. A.; Schneider, H.; Glöss, A.; Weber, J. M. An infrared investigation of the $(CO_2)_n^-$ clusters: Core ion switching from both the ion and solvent perspectives. *J. Phys. Chem. A* **2005**, *109*, 3146−3152.
(35) Klots, C. E. Evaporative cooling. *J. Chem. Phys.* **1985**, *83*, 5854−5860.
(36) Fatur, S. M.; Shepard, S. G.; Higgins, R. F.; Shores, M. P.; Damrauer, N. H. A synthetically tunable system to control MLCT excited-state lifetimes and spin states in iron(II) polypyridines. *J. Am. Chem. Soc.* **2017**, *139*, 4493−4505.
(37) Walsh, A. D. 467. The electronic orbitals, shapes, and spectra of polyatomic molecules. Part II. Non-hydride AB2 and BAC molecules. *J. Chem. Soc.* **1953**, 2266−2288.

DOI: 10.1021/acs.jpca.7b02742
J. Phys. Chem. A 2017, 121, 4132−4138